Development 135, 4141-4151 (2008) doi:10.1242/dev.027912

γ-Protocadherins regulate neuronal survival but are dispensable for circuit formation in retina

Julie L. Lefebvre[1], Yifeng Zhang[1], Markus Meister[1], Xiaozhong Wang[2] and Joshua R. Sanes[1,*]

Twenty-two tandemly arranged protocadherin-γ (Pcdh-γ) genes encode transmembrane proteins with distinct cadherin-related extracellular domains and a common intracellular domain. Genetic studies have implicated Pcdh-γ genes in the regulation of neuronal survival and synapse formation. Because mice lacking the Pcdh-γ cluster die perinatally, we generated conditional mutants to analyze roles of Pcdh-γ genes in the development and function of neural circuits. Retina-specific deletion of Pcdh-γs led to accentuation of naturally occurring death of interneurons and retinal ganglion cells (RGCs) during the first two postnatal weeks. Nonetheless, many neuronal subtypes formed lamina-specific arbors. Blocking apoptosis by deletion of the pro-apoptotic gene *Bax* showed that even neurons destined to die formed qualitatively and quantitatively appropriate connections. Moreover, electrophysiological analysis indicated that processing of visual information was largely normal in the absence of Pcdh-γ genes. These results suggest that Pcdh-γ genes are dispensable for elaboration of specific connections in retina, but play a primary role in sculpting neuronal populations to appropriate sizes or proportions during the period of naturally occurring cell death.

KEY WORDS: Apoptosis, Interneuron, Laminar specificity, Receptive field, Mouse

INTRODUCTION

The assembly of neurons into complex stereotyped circuits has been hypothesized to require large sets of cell-surface molecules that mediate cell-cell interactions. A group of genes called clustered protocadherins (Pcdhs) has intriguing features that suggest their involvement in these processes. First, they have a remarkable genomic organization in which 58 homologous genes are arranged in three subclusters (Pcdh-α, -β and -γ) arrayed in tandem on a single chromosome (Kohmura et al., 1998; Obata et al., 1998; Wu and Maniatis, 1999; Wu and Maniatis, 2000). Second, α- and γ-protocadherins arise through the combination of distinct extracellular domains with a common cytoplasmic domain, suggesting a mechanism in which distinct recognition events promote a common cellular response. Third, Pcdhs are members of the cadherin superfamily, other members of which mediate selective intercellular interactions, including synapse formation (Takeichi, 2007). Fourth, Pcdhs are expressed predominantly in the nervous system, with individual family members expressed in combinatorial patterns (Esumi et al., 2005; Frank et al., 2005; Kohmura et al., 1998; Zou et al., 2007). Fifth, Pcdh proteins are associated at least in part with synaptic membranes (Kohmura et al., 1998; Phillips et al., 2003; Wang et al., 2002). Finally, clustered protocadherin orthologs are present in vertebrates but not in invertebrates (Hill et al., 2001; Hirayama and Yagi, 2006; Noonan et al., 2004). Together, these features suggest that Pcdhs might underlie complex patterns of selective neural connectivity in vertebrates.

The first genetic test of this hypothesis led to an unexpected result: targeted mouse mutants lacking all 22 Pcdh-γ genes exhibited massive apoptosis of spinal interneurons during late fetal life and died within hours of birth (Wang et al., 2002). Synapse number was also reduced in mutant spinal cords. This was not a trivial consequence of decreased neuronal number, as synaptic defects and perinatal lethality persisted when apoptosis was blocked (Weiner et al., 2005). Thus, neural connectivity may be defective in the absence of Pcdh-γ genes, and apoptosis may be secondary to circuit defects. However, the associated lethality and the complexity of spinal circuitry have made it difficult to test these possibilities. In addition, it remains unknown whether Pcdh-γ genes are required for neuronal survival and synaptogenesis in other regions of the nervous system.

To address these issues, we generated conditional alleles of the Pcdh-γ cluster, restricting inactivation to defined neuronal populations and bypassing neonatal lethality. Here, we focus on the retina, which has several advantages, including a stereotyped structure, markers for many neuronal and synaptic subtypes, and a clear understanding of the tissue's function (Masland, 2001; Wässle, 2004). We used Cre recombinase to delete Pcdh-γ genes from retinal neurons and glia, and assessed the consequences for neuronal structure and function. Surprisingly, lamina-specific arbors and complex functional circuits formed in the absence of Pcdh-γ genes, suggesting that these genes play limited roles in synaptic specificity. By contrast, loss of Pcdh-γ genes accentuated naturally occurring death of multiple retinal cell types. These results suggest a primary role for Pcdh-γ genes in neuronal population matching during development.

MATERIALS AND METHODS

Animals/generation of targeted mice

Pcdh-γ^{fusg} and *Pcdh-γ^{del}* mutants have been described previously (Wang et al., 2002). Mice in which regulatory elements from the *Chx10* gene drive expression of a Cre-GFP fusion protein linked by an internal ribosome entry site (IRES) to placental alkaline phosphatase (*Chx10-Cre*) (Rowan and Cepko, 2004) were provided by Constance Cepko (Harvard). Mice in which a short enhancer fragment from the *Pax6* gene drive expression of a Cre-IRES-GFP cassette (*Pax*α*-Cre*) (Marquardt et al., 2001) were provided by Peter Gruss (Göttingen, Germany). Mice in which regulatory elements from the β-actin gene drive expression of Cre (*Actin-Cre*) (Lewandoski et al., 1997) were provided by Gail Martin (UCSF). *Bax* mutants (Knudson et al., 1995) and Z/EG reporter mice (Novak et al., 2000) were obtained from Jackson Laboratories.

[1]Department of Molecular and Cellular Biology and Center for Brain Science, Harvard University, Cambridge, MA 02138, USA. [2]Department of Biochemistry, Molecular Biology and Cell Biology, Northwestern University, Evanston, IL 60208, USA.

*Author for correspondence (e-mail: sanesj@mcb.harvard.edu)

Accepted 24 September 2008

The *Pcdh-γ*^{fcon3} targeting vector was modified from the *Pcdh-γ*^{fusg} vector shown in Fig. 2B of Wang et al. (Wang et al., 2002) by inserting a loxP sequence into an *Nhe*I site upstream of the final coding exon. The *Pcdh-γ*^{fdel} allele was generated by re-targeting the ES cells used to generate *Pcdh-γ*^{fusg} with the vector that had been used to generate *Pcdh-γ*^{del}. This vector inserted a loxP sequence directly upstream of variable exon A1. Homologous recombinants and germ line chimeras were generated by standard methods. Mice were maintained on a C57/B6J background.

Histology

Mice were euthanized with intraperitoneal injection of Nembutal and eye cups were fixed in 4% paraformaldehyde. Tissue was cryoprotected in sucrose, frozen and sectioned at 20 μm in a cryostat. Slides were incubated successively with blocking solution, primary antibodies (12-16 hours at 4°C) and Alexa Fluor-conjugated secondary antibodies (Invitrogen; 3 hours at room temperature). Primary antibodies were: anti-GFP (Aves and Chemicon); anti-calbindin (Swant); anti-choline acetyltransferase (Chemicon); anti-protein kinase Cα (AbCam); anti-neurokinin receptor 3 (Calbiochem); anti-synaptotagmin II (Zebrafish International Resource Center); anti-disabled 1 (a gift from T. Curran); anti-Gγ13 (Santa Cruz); anti-Bassoon (Stressgen); anti-synaptophysin (Zymed); anti-Chx10 (Exalpha Biologicals); anti-Sox9 (Chemicon); anti-glutamine synthetase (BD Biosciences); anti-cleaved caspase 3 (Cell Signaling Technology); anti-Brn3a (Chemicon); anti-VGlut3 (Chemicon); anti-syntaxin (Sigma); anti-Thy1.2 (BD Pharmingen); anti-GlyT1 (Santa Cruz); and anti-tyrosine hydroxylase (Chemicon). Peanut agglutinin was from Invitrogen. Nuclei were labeled with DAPI, Po-pro1 or NeuroTrace Nissl 435/455 (Invitrogen).

For measurements of retinal layer thickness and cell number, areas were chosen at equivalent retinal eccentricities from the optic nerve head or ora serrata. Layer thickness was measured on single optical sections, adjacent to the optic nerve head. Two to four areas were measured from each retina and two sets of perpendicular measurements were made per area. Both *Chx10-Cre;Pcdh-γ*$^{fcon3/+}$ and *Pcdh-γ*$^{fcon3/+}$ littermates were used as controls for *Chx10-Cre;Pcdh-γ*$^{fcon3/fcon3}$ mutants, and similarly for *Pcdh-γ*^{fdel}. Immunolabeled cells were quantified from 0.13 mm^2 (calbindin, ChAT, Brn3a and Paxα-GFP), 0.05 mm^2 (Chx10), 0.02 mm^2 (Sox9) or 1280 μm^2 (photoreceptors) optical sections. Apoptotic cells were counted on sections spanning the optic nerve head to the ora serrata. Cells were classified as apoptotic if cleaved caspase 3 immunoreactivity partially or completely surrounded a nucleus. Means were compared using ANOVA, Student's *t*-test on condition of equivalent variances determined by F-test or with Mann-Whitney non-parametric test.

In situ hybridization of retinal sections was performed as described previously (Wang et al., 2002).

Retinas were dissociated with papain by a modification of the protocol described by Meyer-Franke et al. (Meyer-Franke et al., 1995). Dissociated cells were plated onto poly-D-lysine coated eight-well Permanox chamber slides (Nunc), then fixed with 4% paraformaldehyde/4% sucrose for 15 minutes, and immunostained. RGCs were enriched with CD90 magnetic Microbeads (Miltenyi-Biotec).

Electrophysiology

Dark-adapted retinas were isolated under an infrared microscope into Ringer's solution at room temperature. A piece of retina, ~3-4 mm in diameter, was placed with RGCs facing down on a 61-electrode array superfused with Ringer's (Kim et al., 2008). Extracellular action potentials were recorded and single units identified by spike-sorting methods as described previously (Meister et al., 1994). White light stimuli were delivered from a computer-driven display projected on the retina.

To map spatio-temporal receptive fields, we projected gratings of adjacent thin bars (8.3 or 16.6 μm width). Each bar flickered black or white according to a pseudo-random binary sequence (16.6 millisecond frame duration). For any given RGC, we computed the spike-triggered average of the flickering bar stimulus (Kim et al., 2008) using

$$h(x,t) = \frac{1}{n}\sum_{j=1}^{n} s\left(x, t_j + t\right) , \quad (1)$$

where $s(x,t)$ is the stimulus intensity at location x and time t, with the time-averaged intensity subtracted, and the neuron fired a total of n spikes at times $\{t_j\}$. Examples are shown in Fig. S2 in the supplementary material.

We then approximated this function as the product of a spatial receptive field $b(x)$ and a temporal integration function $a(t)$:

$$h(x,t) \approx b(x) \times a(t) \quad (2)$$

These are the spatial and temporal components analyzed in Fig. 9. For analysis of response threshold and gain, we fitted the time-dependent RGC firing rate $r(t)$ by a linear-nonlinear model (Chichilnisky, 2001):

$$r(t) = N\left(y(t)\right)$$
$$y(t) = \frac{1}{Z}\int s(x,t')\,h(x,t'-t)\,dt' , \quad (3)$$

where Z is chosen so that $y(t)$ has unit variance, and

$$N(y) = \begin{cases} B, & \text{if } y < \theta \\ B + G \cdot y, & \text{if } y > \theta \end{cases}$$

is a rectifying function with threshold θ and gain G.

RESULTS

Broad expression of gamma protocadherins in retina

We began our study by assessing the distribution of Pcdh-γ genes in retina. We used targeted mutant mice in which GFP is fused to the shared C terminus, tagging all 22 Pcdh-γ isoforms (Pcdh-γ^{fusg}) (Wang et al., 2002). Homozygous *Pcdh-γ*$^{fusg/fusg}$ mutants are viable and fertile, and show none of the defects documented previously in *Pcdh-γ* mutants (Wang et al., 2002; Weiner et al., 2005). We therefore believe that GFP is a neutral reporter of endogenous Pcdh-γ localization.

The retina consists of three cellular layers separated by two synaptic or 'plexiform' layers (Fig. 1A). The cellular layers are the outer nuclear layer (ONL), containing photoreceptors; the inner nuclear layer (INL), containing interneurons (horizontal, bipolar and amacrine cells) and Müller glia; and the ganglion cell layer (GCL), containing RGCs and displaced amacrine cells. The outer plexiform layer (OPL) contains synapses of photoreceptors onto horizontal and bipolar cells, and the inner plexiform layer (IPL) contains synapses of bipolar and amacrine cells onto RGCs. As judged by localization of GFP in *Pcdh-γ*^{fusg} mice, Pcdh-γs are present in all five retinal layers (Fig. 1A). In the ONL, Pcdh-γs are present in outer segments and around photoreceptor somata (Fig. 1B); in the INL and GCL, Pcdh-γs outline neuronal somata (Fig. 1C,D). Pcdh-γ levels are highest in the most membrane-rich layers: IPL, OPL and the optic fiber layers that carry RGC axons to the brain (Fig. 1A′,D). In situ hybridization confirmed Pcdh-γ expression by cells in the INL and GCL, though this method did not reliably detect *Pcdh-γ*RNA in photoreceptors (Fig. 1E).

To determine which retinal cell types express *Pcdh-γ* genes, we dissociated *Pcdh-γ*^{fusg} retinas and immunostained cells with antibodies to cell-type-specific markers (Haverkamp and Wässle, 2000; Wahlin et al., 2004; Zhang et al., 2004). This method circumvented the difficulty of determining which of the cells abutting Pcdh-γ-rich membranes are themselves Pcdh-γ positive. Markers included Brn3a and Thy1 for RGCs, syntaxin 1 for amacrine cells, Chx10 for bipolar cells, calbindin for horizontal cells, recoverin for photoreceptors and glial fibrillary acidic protein, Sox9 and glutamine synthetase for Müller glia. All six cell types were Pcdh-γ positive (Fig. 1F-K; data not shown). Thus, Pcdh-γs are expressed in all cell types of the neural retina.

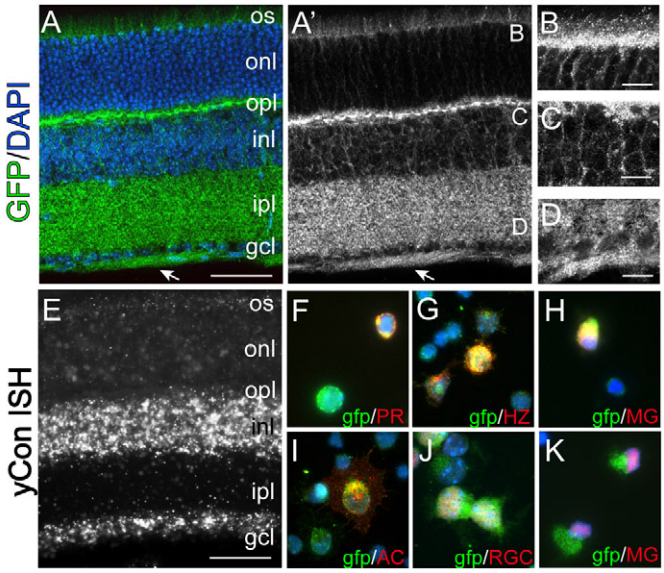

Fig. 1. Pcdh-γ genes are broadly expressed in the retina. (**A-D**) Retinas from *Pcdh-γ*$^{fusg/fusg}$ mice, expressing a Pcdh-γ-GFP fusion protein, were stained with antibody to GFP (green in A) and DAPI (blue in A). Pcdh-γ-GFP fusion proteins are concentrated in the process-rich outer plexiform layer (OPL), inner plexiform layer (IPL) and retinal fiber layer (arrow), as well as in outer segments (OS) of photoreceptors, outer and inner nuclear layers (ONL, INL) and the ganglion cell layer (GCL). (B-D) High-magnification images of areas labeled in A′. (**E**) In situ hybridization to P21 retina using a probe against the Pcdh-γ common intracellular domain. (**F-K**) Dissociated *Pcdh-γ*$^{fusg/fusg}$ retinal cells immunolabeled with cell-type-specific antibodies (red), anti-GFP (green) and DAPI (blue). Pcdh-γ-GFP-positive cells are labeled with the photoreceptor (PR) marker recoverin, the horizontal cell (HZ) marker calbindin, the amacrine (AC) marker syntaxin, the RGC marker Brn3a, and the Müller Glia (MG) markers glutamine synthetase (H) and Sox9 (K). Scale bars: 50 μm in A,E; 10 μm in B-D.

We asked whether Pcdh-γ genes are present in the retina during early postnatal life, when neural circuits form. At postnatal day (P) 0, the retina contains ganglion cell and neuroblast layers, separated by a nascent IPL. All RGCs have been born by this time, while neurogenesis and migration of newborn interneurons and photoreceptors continue in the neuroblast layer. At this time, Pcdh-γ is present on cells in the neuroblast layer, in the IPL, and on RGC axons (Fig. 2A). At P3, Pcdh-γ is apparent in the layer of horizontal cells that prefigures the OPL (Fig. 2B). By P7, Pcdh-γ appears in the OPL, as it divides the neuroblast layer into INL and ONL (Fig. 2C). By P14, the adult pattern described above is established (Fig. 2D).

Synaptic localization of Pcdh-γ proteins in the retina

To evaluate the subcellular localization of Pcdh-γ proteins, we focused on the OPL, because its synapses are larger than those in the IPL. We labeled photoreceptor terminals with antibodies to bassoon, which is present in both rod terminals (spherules) and cone terminals (pedicles), and labeled spherules and pedicles selectively with anti-PSD-95 and peanut agglutinin, respectively (Blanks et al., 1987; Koulen et al., 1998; tom Dieck and Brandstätter, 2006). Pcdh-γ was associated with both spherules and pedicles (Fig. 3A-C). We labeled bipolar cell dendrites with antibodies to protein kinase Cα and neurokinin receptor 3, which mark rod and cone bipolars, respectively, and to G protein γ13 (Gγ13), which is present in subsets of both rod and cone bipolars (Haverkamp et al., 2003; Huang et al., 2003). Pcdh-γ was associated with both rod and cone bipolar dendrites (Fig. 3D; data not shown). Thus, Pcdh-γ genes were present in pre- and postsynaptic compartments of rod and cone synapses. By contrast, although horizontal cell processes labeled with anti-calbindin (Sharma et al., 2003) were Pcdh-γ positive, little Pcdh-γ was present in their synaptic varicosities (Fig. 3E).

Pcdh-γ was also present throughout the IPL. GFP-positive puncta often overlapped with bassoon-positive presynaptic ribbons in bipolar cells, glutamate decarboxylase- and GlyT1-positive terminals of inhibitory amacrines, and PSD-95-positive postsynaptic membranes of excitatory synapses (Fig. 3F; data not shown). Taken together, these results suggest that Pcdh-γs are present at many synapses in the retina, although they are not confined to synapses.

Inactivation of Pcdh-γs in the retina leads to neuronal and synaptic loss

Pcdh-γ null and hypomorphic mice die shortly after birth (Wang et al., 2002; Weiner et al., 2005). We examined retinas of *Pcdh-γ* null mutants at late embryonic stages [embryonic day (E) 17-18; birth is at E19] but found no obvious defects in retinal structure (see below). However, as the development of retinal circuitry occurs largely during postnatal life, roles of Pcdh-γ in circuit formation and function could not be studied in these mutants. We therefore

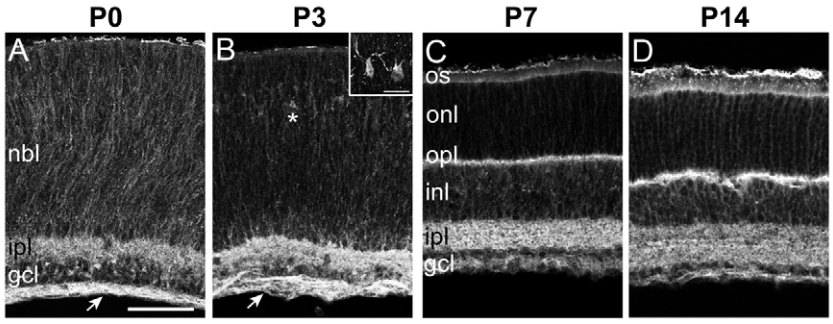

Fig. 2. Pcdh-γ proteins localize to retinal plexiform layers during postnatal development. (**A-D**) Immunolabeling of *Pcdh-γ*$^{fusg/fusg}$ retina at P0 (A), P3 (B), P7 (C) and P14 (D) with GFP antibody. At P0 (A) and P3 (B), Pcdh-γ-GFP proteins are present in the IPL and retinal axon layer (arrow), and are distributed around cell somata in the neuroblast layer (NBL; other abbreviations as in Fig. 1). At P3, Pcdh-γ proteins are also present in presumptive horizontal cells (asterisk; inset in B). (C) By P7, Pcdh-γ-GFPs are detected in the emerging OPL, as it develops between the ONL and INL. (D) By P14, the adult pattern of Pcdh-γ-GFP localization (see Fig. 1) is attained. Scale bars: 20 μm in A; 10 μm in inset.

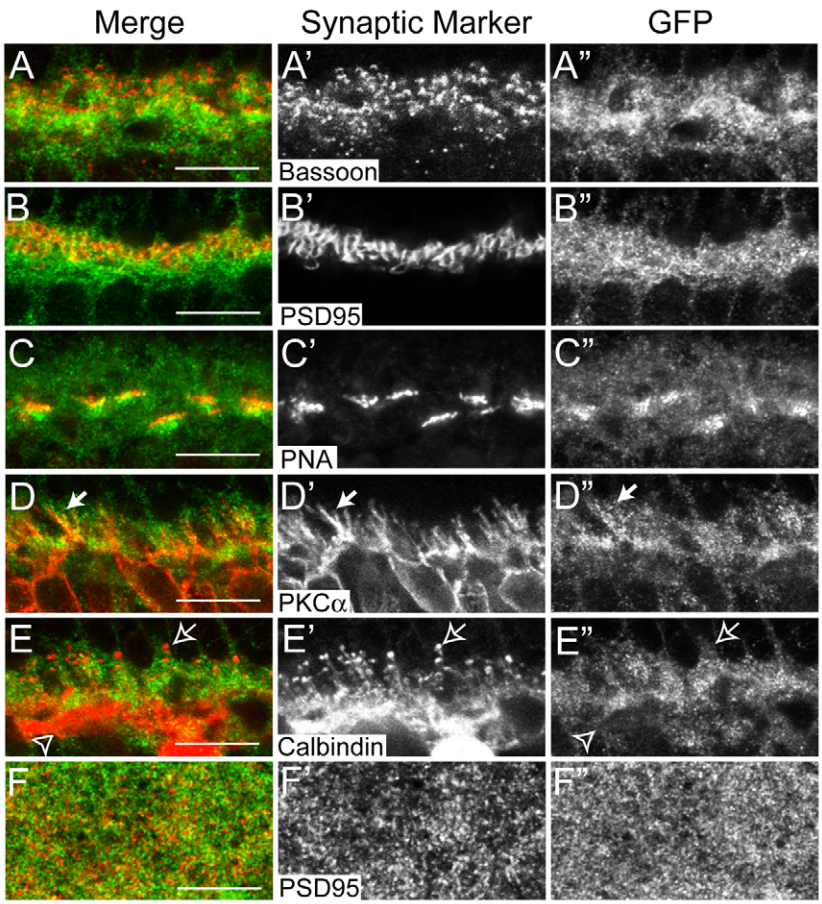

Fig. 3. Subcellular localization of Pcdh-γ proteins in the synaptic plexiform layers. (A-E) Confocal images of the OPL of *Pcdh-γ*$^{fusg/fusg}$ retinas double labeled with anti-GFP (green) and antibodies against proteins present in the synapses that photoreceptors form on horizontal and bipolar cells (red). (**A**) Bassoon, a component of synaptic ribbons in all photoreceptor nerve terminals. (**B**) PSD-95, a component of rod terminals (spherules). (**C**) Peanut agglutinin (PNA) labels cone terminals (pedicles). (**D**) PKCα, a component of rod bipolar dendrites (arrow). (**E**) Calbindin, a component of horizontal cell processes (open arrow) that terminate onto rod spherules as well as horizontal cell processes that stratify in the inner OPL (open arrowhead). Pcdh-γ proteins are present in both spherules and pedicles, and in bipolar and amacrine processes, but are not seen in horizontal cell varicosities (open arrow). (**F**) A single confocal plane of the IPL of *Pcdh-γ*$^{fusg/fusg}$ retinas labeled with anti-GFP (green) and antibodies to PSD-95 (red), which marks excitatory postsynaptic sites in this lamina. Fine Pcdh-γ-GFP puncta are distributed throughout the IPL, and are present at but not restricted to synapses. Scale bars: 10 μm.

generated two conditional inactivation alleles to bypass neonatal lethality (Fig. 4A). In *Pcdh-γ*^{fdel}, loxP sites flank the entire *Pcdh-γ* locus, such that Cre-mediated recombination generates a null allele. In *Pcdh-γ*^{fcon3}, the C-terminal exon shared by all isoforms is flanked by loxP sites, such that Cre truncates all Pcdh-γ genes. In both alleles, GFP is fused to this C-terminal exon, allowing us to use loss of GFP as an indicator of Cre-mediated Pcdh-γ excision. The Pcdh-γ-GFP fusion protein was identical to that in the *Pcdh-γ*^{fusg} allele described above.

In initial tests, we excised the floxed segments of the *Pcdh-γ*^{fdel} and *Pcdh-γ*^{fcon3} alleles in the germline by mating them to transgenic mice in which Cre is expressed ubiquitously (*Actin-Cre*) (Lewandoski et al., 1997). Homozygotes generated from these animals died at birth and exhibited spinal cord phenotypes similar to those described previously in null mutants (Wang et al., 2002), indicating that recombination inactivates the *Pcdh-γ* gene (data not shown). Western blotting reported by Prasad et al. (Prasad et al., 2008) failed to detect Pcdh-γ protein in *Actin-Cre;Pcdh-γ*$^{fcon3/fcon3}$ mice, indicating that this allele is effectively a protein null. The truncation in *Pcdh-γ*^{fcon3} is more extensive than the hypomorphic allele described previously (*Pcdh-γ*^{tr}), in which Pcdh-γ levels were decreased several-fold (Weiner et al., 2005). We speculate that increased truncation of *Pcdh-γ*^{fcon3} and lack of a polyadenylation signal led to greater destabilization of *Pcdh-γ* protein and mRNA, respectively.

To selectively inactivate Pcdh-γs in retina, we crossed *Pcdh-γ*^{fdel} and *Pcdh-γ*^{fcon3} mutants with mice in which a GFP-Cre recombinase fusion protein is expressed under the control of regulatory elements from the *Chx10* gene (*Chx10-Cre*) (Rowan and Cepko, 2004). These elements drive expression of GFP-Cre transiently in embryonic retinal progenitors and postnatally in bipolar cells. To assay recombination in retinas of *Chx10-Cre* mice, we crossed them to a reporter line in which β-galactosidase (*lacZ*) and GFP label non-recombined and recombined cells, respectively (Z/EG) (Novak et al., 2000). Recombination was extensive (>90%) in the INL and ONL, but occasional columns of cells were spared (see Fig. S1A in the supplementary material). By contrast, approximately half of the cells in the GCL were GFP-negative and *lacZ* positive (see Fig. S1B in the supplementary material). This pattern may reflect the fact that many RGCs are born by E12 (Farah and Easter, 2005), before Cre accumulates in progenitors. We then used *loss* of GFP to assay Chx10-Cre-mediated loss of Pcdh-γ-GFP from the *Pcdh-γ* alleles. This method did not allow us to assess excision in bipolars, in which GFP was expressed from the Chx10 transgene (see Materials and methods). Nonetheless, Chx10-Cre excised *Pcdh-γ*^{fdel}, *Pcdh-γ*^{fcon3} and Z/EG genes in similar patterns and to a similar extent (see Fig. S1C-E in the supplementary material). The efficacious excision of the *Pcdh-γ*^{fdel} allele is surprising given the length of the floxed segment.

Chx10-Cre;Pcdh-γ$^{fdel/fdel}$ mice are healthy and outwardly normal. We first examined these mutants at P18, by which time the retinal architecture is well developed. Labeling of nuclear layers with DAPI and plexiform layers with antibodies to the synaptic vesicle protein synaptophysin revealed that mutant retinas were properly laminated (Fig. 4B-G). However, mutant retinas were ~25% thinner than those of wild-type mice or heterozygote littermates. The difference resulted from a selective reduction of ~40% in the thickness of the INL and the IPL (Fig. 4H). Thus, Pcdh-γs are required for

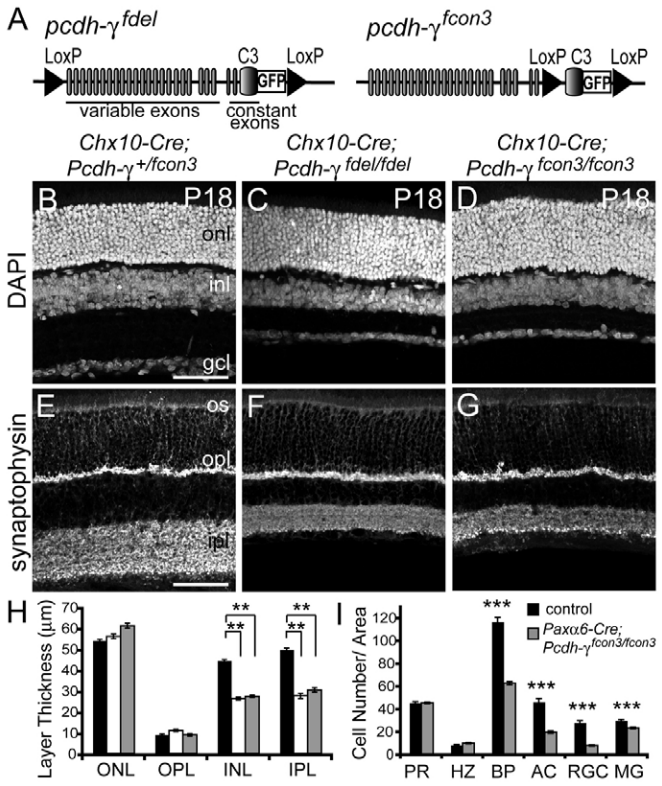

Fig. 4. Thinned INL and IPL in retinae lacking Pcdh-γ proteins. (**A**) Diagram of conditional *Pcdh-γ* inactivation alleles. Each Pcdh-γ protein is encoded by an mRNA, comprising one of 22 variable exons and the three constant 'C' exons. In *Pcdh-γ*^{fdel}, loxP sites flanking the entire *Pcdh-γ* locus result in deletion of all *Pcdh-γ* genes upon Cre-mediated recombination. In *Pcdh-γ*^{fcon3}, loxP sites flank the final C3-GFP exon, resulting in truncated forms of Pcdh-γ proteins. In both alleles, GFP is fused to the C terminus of the C3 exon. (**B-G**) Sections from P18 control and *Pcdh-γ*-deficient retinas, labeled with DAPI or anti-synaptophysin to highlight nuclear and synaptic layers, respectively. Retinal lamination is normal, and OPL and ONL are normal in thickness but IPL and INL are markedly thinned in mutants. (**H**) Quantification of nuclear and plexiform layer thickness in control (black), *Chx10-Cre; Pcdh-γ*$^{fdel/fdel}$ (white) and *Chx10-Cre;Pcdh-γ*$^{fcon3/fcon3}$ (gray) retinas at P18. Bars show mean±s.e.m. from three or four animals of each genotype. ***P<0.01*, ANOVA and post-hoc Tukey test. (**I**) Quantification of retinal cell types in *Pax6α-Cre;Pcdh-γ*$^{+/fcon3}$ (black) and *Pax6α-Cre;Pcdh-γ*$^{fcon3/fcon3}$ (gray) P18 retinas. Bars show mean±s.e.m. from six to eight animals of each genotype. PR, photoreceptors by Po-pro1; HZ, calbindin+ horizontal cells; BP, Chx10+ bipolar cells; AC, Pax6α+ amacrines; RGC, Brn3a+ retinal ganglion cells; MG, Sox9+ Müller Glia. Other abbreviations as in Fig. 1. Error bars indicate s.e.m. ***P*<0.0001, Mann-Whitney non-parametric test. Scale bars: 50 μm.

development or maintenance of retinal interneurons and the layer in which they form synapses. The INL and IPL were thinned to the same extent in *Chx10-Cre;Pcdh-γ*$^{fcon3/fcon3}$ and *Chx10-Cre;Pcdh-γ*$^{fdel/fdel}$ mice (Fig. 4C,D,F,G), consistent with the idea that *Pcdh-γ*^{fcon3} is functionally a null. In subsequent studies, we used the two alleles interchangeably, but most of the results reported here are from *Pcdh-γ*^{fcon3} mice.

The mosaicism described above for *Chx10-Cre* retinas made quantification of cell loss imprecise in the GCL. We therefore used a second transgenic line, *Pax6α-Cre*, in which Cre is expressed under the control of retina-specific sequences from the *Pax6* gene (Marquardt et al., 2001). The *Pax6α-Cre* transgene drives expression of Cre transiently in embryonic retinal progenitors, leading to essentially complete (>99%) inactivation in peripheral retina; a sector in central retina is spared, as described below. Postnatally, *Pax6α-Cre* is expressed in a subset of amacrines, which can be identified by a GFP reporter within the transgene.

We used cell type-specific markers (see above) to quantify cell loss from peripheral regions of *Pax6α-Cre;Pcdh-γ*$^{fcon3/fcon3}$ retinas at P18. Numbers of bipolar, amacrine and retinal ganglion cells were reduced by 45-65% (Fig. 4I). Müller glia were also decreased, but only by ~20%. By contrast, numbers of horizontal cells and photoreceptors differed little between mutants and controls (Fig. 4I). Together, these results demonstrate that Pcdh-γ genes are essential for the survival of many but not all retinal cell types.

Increased postnatal apoptosis in the absence of Pcdh-γ genes

We next asked when retinal defects arise in *Pcdh-γ* mutants, and whether they are progressive. We detected no differences in laminar arrangement or thickness between mutant and control retinas perinatally (E17.5-P3) (Fig. 5A,B,G,H and data not shown). By P7, however, shortly after the ONL and INL form, mutant retinas were thinner than those of controls (Fig. 5C,D). We used *Chx10-Cre; Pcdh-γ*^{fcon3} mice for quantification of these defects. Both layers were ~40% thinner in mutants than in controls by P14, then changed little over the following months (Fig. 5E-I). Thus, the difference between mutant and control retinas appears during the first postnatal week, is maximal by the end of the second postnatal week, and neither abates nor worsens substantially thereafter.

A process of naturally occurring programmed cell death eliminates many retinal neurons during the first two postnatal weeks (Pequignot et al., 2003; Young, 1984). Apoptosis followed a similar time course in Pcdh-γ deficient retinas, but levels were significantly higher in mutants than in controls (Fig. 5J-L). Although increased apoptosis was seen in both neuroblast and ganglion cell layers at P0, it was confined to the INL at P7 (Fig. 5M). This pattern is consistent with the finding that naturally occurring cell death in the GCL is complete several days before that in the INL (Farah and Easter, 2005; Pequignot et al., 2003; Young, 1984). These results suggest that Pcdh-γ genes regulate neuronal survival during the period of naturally occurring programmed cell death.

Cell autonomy of Pcdh-γ-dependent cell survival in retina

Are Pcdh-γ genes required for cell survival in cells that express them, in neighboring cells, or in both? As a first step to distinguish between these possibilities, we capitalized on the recombination pattern in *Pax6α-Cre* transgenic mice. As noted above, Cre is expressed in all progenitors in peripheral retina as well as in a subset of amacrine cells marked by the GFP in the transgene. In a large dorsoventrally oriented swath of central retina, however, Cre is expressed in amacrines but not progenitors (Marquardt et al., 2001; Stacy et al., 2005). Thus, in central retina of *Pax6α-Cre;Pcdh-γ*$^{fcon3/fcon3}$ mice, GFP-positive amacrine cells lack Pcdh-γ genes, whereas all other cells, including Müller glia, are Pcdh-γ positive (Fig. 6A-E).

We asked whether Pax6α-positive (that is, GFP-positive) amacrines were lost from central retina of *Pax6α-Cre;Pcdh-γ*$^{fcon3/fcon3}$ mice, despite being surrounded by Pcdh-γ-positive cells. The number of Pax6α-amacrines in central retina was 58% lower in mutants than in controls (Fig. 6B,C,F). Because multiple,

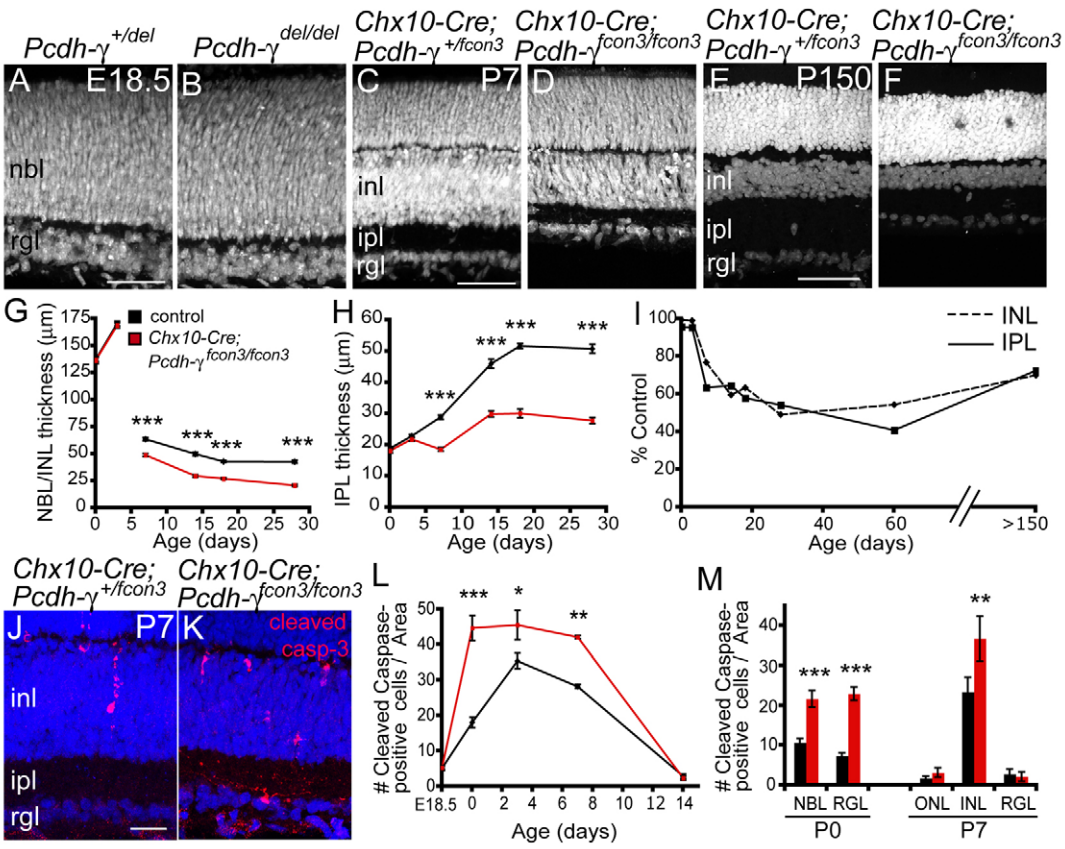

Fig. 5. Thinning of Pcdh-γ mutant retina reflects increased apoptosis during a restricted postnatal period. (**A-F**) Nuclear labeling of Pcdh-$\gamma^{del/del}$, *Pcdh-*$\gamma^{fcon3/fcon3}$, and control retinas at E18.5 (A,B), P7 (C,D) and P15.0 (E,F). Mutant and control retinas are indistinguishable at E18.5 but INL and IPL are thinner in mutant retinas than in controls by P7. Although the INL becomes thinner in both mutants and controls over the subsequent 5 months, the difference between them is not progressive. (**G**,**H**) Thickness of NBL/INL (NBL at P0 and P3, INL at later stages) and IPL in control (black) and *Chx10-Cre;Pcdh-*$\gamma^{fcon3/fcon3}$ mutant retina sections (red). The mutant NBL/INL and IPL develop normally through P3, then decline in thickness relative to controls over the next few weeks. Graphs show mean±s.e.m. from three or four animals. ***P<0.001, Student's t-test. (**I**) NBL/INL and IPL thickness in *Pcdh-*$\gamma^{fcon3/fcon}$ mutant retinas, expressed as percentage of control. (**J**,**K**) Increased numbers of apoptotic cells, marked by cleaved caspase 3 immunoreactivity (red), in *Pcdh-*$\gamma^{fcon3/fcon3}$ mutant retinas at P7 compared with controls. (**L**,**M**) Quantification of cleaved caspase 3 immunopositive cells in control (black) and *Pcdh-*$\gamma^{fcon3/fcon3}$ mutant (red) retinas. Differences between genotypes are significant in the NBL/IPL at P0 and P7, but in the ganglion cell layer only at P7. Results from three to six animals per stage. ***P<0.001; **P<0.01; *P<0.05; Student's t-test or Mann-Whitney test. Abbreviations as in Fig. 1. Scale bars: 20 μm.

neighboring amacrines are Pcdh-γ deficient in the central region, this result does not demonstrate cell autonomy sensu strictu, but does indicate that loss of Pcdh-γ genes from a single cell type impairs its survival, even when the majority of its synaptic inputs (bipolar cells) and targets (RGCs) are wild type. This result also rules out the possibility that neuronal apoptosis in the absence of Pcdh-γ is secondary to a defect in surrounding glial cells. Furthermore, loss of Pax6α-positive amacrines is equivalent in peripheral and central retina (Fig. 6F), indicating that Pcdh-γ-negative cells are not protected from apoptosis when surrounded by Pcdh-γ-positive cells.

We also asked whether loss of Pcdh-γs from Pax6α-amacrines was detrimental to survival of neighboring cells (Fig. 6F). Loss of Pcdh-γs from the Pax6α-positive amacrines had no detectable effect on the survival of bipolar cells, horizontal cells or Müller glia. Likewise, survival of a distinct, intermingled subpopulation of amacrines – the cholinergic starburst cells – was unaffected in central retina. By contrast, we detected a small (~15%) but significant loss of Brn3a-positive RGCs from central retina of *Pax6α-Cre;Pcdh*$\gamma^{fcon3/fcon3}$ mice. We do not know whether this loss reflects absence of Pcdh-γs per se, or death of amacrines, which regulate at least some aspects of RGC development (Goldberg et al., 2002).

Pcdh-γ genes are dispensable for laminar targeting of retinal neurons

Although the width of the IPL is dramatically reduced in Pcdh-γ-deficient retina, it nonetheless contains synapses, as judged by the presence of pre- and postsynaptic markers such as synaptophysin and bassoon (Fig. 4E-G; Fig. 8A,B). Are they appropriate synapses? The retina is well-suited to test specificity, because discrete subsets of bipolar and amacrine cells arborize and synapse in just one or a few of at least 10 closely spaced parallel sublaminae within the IPL (Pang et al., 2002; Roska and Werblin, 2001; Wässle, 2004).

We used markers of 10 lamina-specified amacrine and bipolar subtypes to assess lamina-specific arborization and connectivity in the absence of Pcdh-γs. We follow a scheme in which five sublaminae of equal width are numbered, from the border of the INL (S1) to the border of the ganglion cell layer (Ghosh et al.,

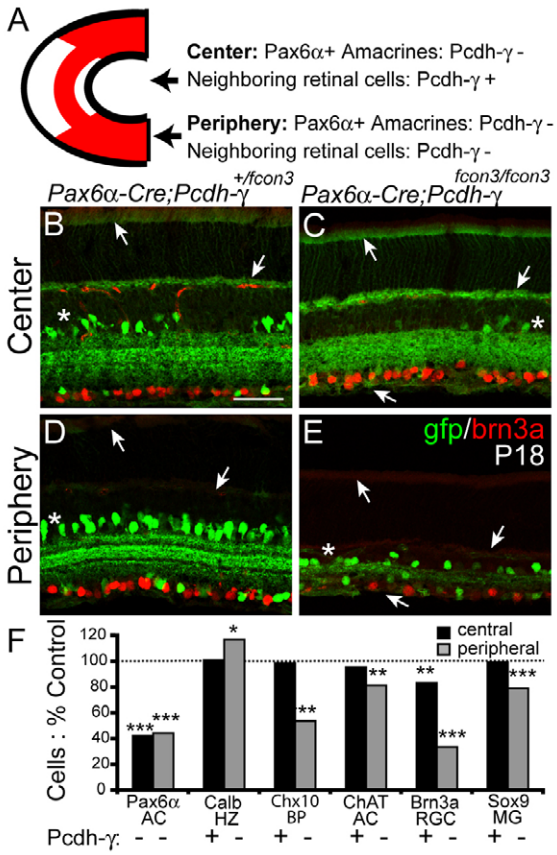

Fig. 6. Cell autonomous and non-autonomous components of Pcdh-γ-dependent cell survival. (**A**) Schematic of the recombination pattern in *Pax6α-Cre* retina. In *Pax6α-Cre;Pcdh-γ*$^{fcon3/fcon3}$ mutants, all cells are *Pcdh-γ* negative in peripheral retina, but only Pax6α-positive (+) amacrine cells are *Pcdh-γ* negative in the central sector. (**B-E**) Immunolabeling of central and peripheral regions of *Pax6α-Cre;Pcdh-γ*$^{+/fcon3}$ and *Pax6α-Cre;Pcdh-γ*$^{fcon3/fcon3}$ mutant retinas with GFP and Brn3a antibodies. Anti-GFP labels both Pax6α-Cre-ires-GFP positive amacrine cells (asterisks) and Pcdh-γ-GFP proteins (arrows). In unrecombined portions of the central *Pax6α-Cre;Pcdh-γ*$^{fcon3/+}$ and *Pax6α-Cre;Pcdh-γ*$^{fcon3/fcon3}$ retinas, Pcdh-γ-GFP proteins are visible in the outer segments, OPL, and retinal axons (arrows). In peripheral regions, Pcdh-γ-GFPs are absent. In both regions, mutant retinas have reduced numbers of Pax6α-positive amacrine cells; Brn3a-positive RGCs are dramatically decreased in the mutant peripheral sector while slightly decreased in the central sector. (**F**) Quantification of retinal cell types in central regions of *Pax6α-Cre;Pcdh-γ*$^{fcon3/fcon3}$ retinas, expressed as a percentage of cells in *Paxα6-Cre;Pcdh-γ*$^{fcon3/+}$ littermates. Six to eight animals per genotype were analyzed; **P*<0.05; ***P*<0.01; ****P*<0.0001, by Student's *t*-test or Mann-Whitney test. Scale bar: 50 μm.

2004; Yamagata and Sanes, 2008). Populations examined were starburst amacrines, labeled by choline acetyltransferase; glutamatergic amacrines (anti-vGlut3); GABAergic amacrines (anti-GAD65/67); dopaminergic amacrines (anti-tyrosine hydroxylase); type AII amacrines (anti-disabled); calbindin-positive amacrines and RGCs; OFF bipolar cells (anti-synaptotagmin 2); ON bipolar cells (anti-Gγ13); OFF bipolars (anti-NK3R); and rod bipolars (anti-protein kinase Cα) (Fig. 7E). In all 10 cases, processes were arrayed in appropriate sublaminae in mutant retinas at P18, although disruptions or gaps were sometimes present (Fig. 7A-D; data not shown). We also observed proper laminar targeting of amacrine subsets at P7, and of bipolar subsets at P14, in each case soon after these synapses formed in controls (data not shown).

Synapses and arbors of Pcdh-γ-deficient neurons destined to die

Results illustrated in Fig. 7 are consistent with the idea that Pcdh-γs are dispensable for formation of neural circuits in retina. Alternatively, however, some INL interneurons might fail to target appropriate sublaminae and then die. In this case, neuronal apoptosis in Pcdh-γ mutants might be secondary to circuit defects. To test this possibility, we blocked apoptosis in *Pcdh-γ*$^{fcon3/fcon3}$ mice by deleting the pro-apoptotic gene, *Bax*. Naturally occurring death in many regions of the nervous system, including retina, is dramatically reduced in *Bax*$^{-/-}$ mice (Mosinger Ogilvie et al., 1998; Pequignot et al., 2003; White et al., 1998), and deletion of *Bax* preserves spinal interneurons that would otherwise die in *Pcdh-γ* null spinal cord (Weiner et al., 2005). Likewise, *Bax* deletion rescued neurons destined to die in *Pcdh-γ* mutant retina: the thickness of the INL and GCL and the number of Chx10-positive bipolar cells were indistinguishable in *Chx10-Cre;Pcdh-γ*$^{+/fcon3}$*;Bax*$^{-/-}$ and *Chx10-Cre;Pcdh-γ*$^{fcon3/fcon3}$*;Bax*$^{-/-}$ retinas (Fig. 8A-D; data not shown).

Deletion of *Bax* also resulted in expansion of the IPL. The IPL in *Chx10-Cre;Pcdh-γ*$^{fcon3/fcon3}$*;Bax*$^{-/-}$ mice was thicker than that in *Pcdh-γ* mutants and indistinguishable from that in Pcdh-γ-positive *Bax*$^{-/-}$ mutants (Fig. 8A-D). The density of synapses in the IPL and OPL, as judged by staining for PNA or bassoon, did not differ significantly between Pcdh-γ-positive and Pcdh-γ-negative *Bax*$^{-/-}$ retinas (Fig. 8E-L; see Fig. S2 in the supplementary material). Thus, loss of Pcdh-γ had little effect on synapse number in the IPL when apoptosis was prevented. This result is consistent with the idea that much of the synapse loss in the IPL of *Pcdh-γ*-deficient retina is a consequence of decreased neuron number.

To assess the laminar targeting of interneurons that would have died in the presence of Bax, we stained *Chx10-Cre;Pcdh-γ*$^{fcon3/fcon3}$*;Bax*$^{-/-}$ retinae with the panel of markers listed above. In all cases, targeting of processes to appropriate laminae was as specific in double mutants as in *Pcdh-γ* single mutants (Fig. 8M,N; data not shown). Moreover, thinning and disruptions of layers observed in *Pcdh-γ* single mutants were rescued in *Pcdh-γ*$^{-/-}$*;Bax*$^{-/-}$ double mutants (compare Fig. 7B,D with Fig. 8M,N). We therefore conclude that the gaps observed in Pcdh-γ deficient retina are secondary to the loss of cells rather than a manifestation of improper laminar targeting.

Functional visual circuits form in the absence of Pcdh-γs

To test whether circuits that form in Pcdh-γ-deficient retina are functional, we recorded light responses from RGCs. These cells integrate signals from amacrine and bipolar interneurons and send the resulting spike trains to the brain. RGCs differ in their responses to visual stimuli, depending on the synaptic inputs they receive. Thus, ON RGCs, which respond primarily to light onset, receive synapses from ON bipolar cells in the inner half of the IPL (nearest the GCL); OFF RGCs receive synapses from OFF bipolars in the outer IPL; and ON-OFF RGCs receive both types of synapses. Further specializations, such as responses that are transient, sustained or selective for moving objects, result from innervation by specific subsets of bipolar and amacrine cells (Masland, 2001; Wässle, 2004). Accordingly, the presence of diverse, specific responses from RGCs is a sensitive indicator of

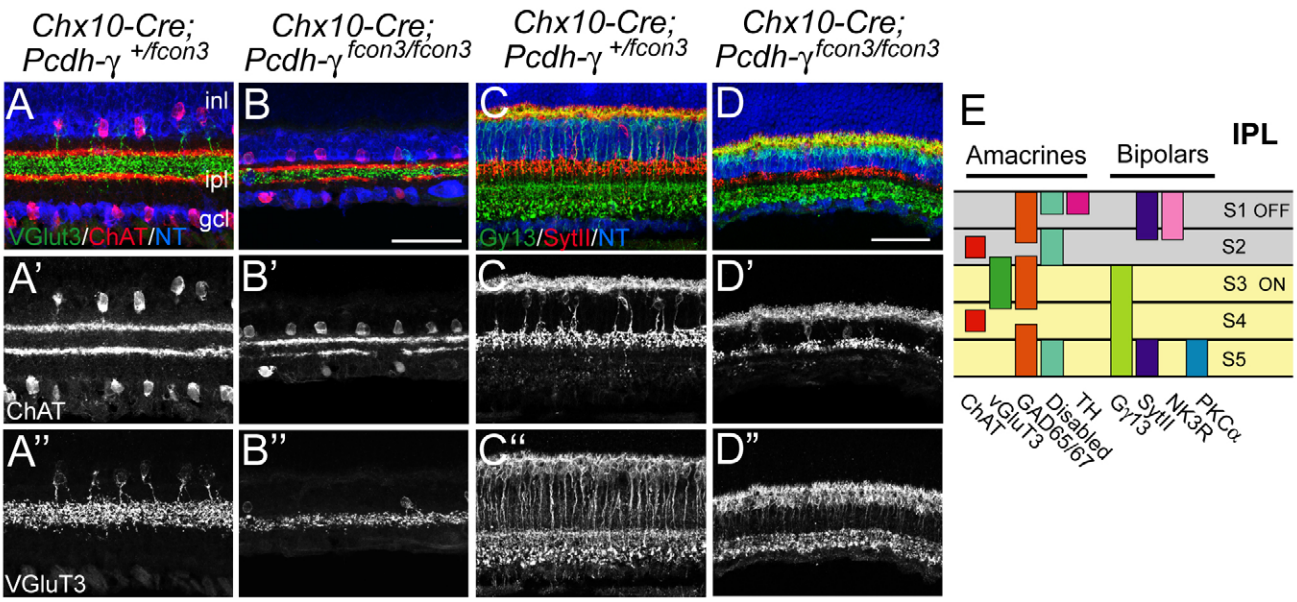

Fig. 7. Sublamina-specific targeting of amacrine and bipolar processes in the IPL in the absence of Pcdh-γ genes. (**A**,**B**) ChAT- (red) and vGluT3-positive amacrine subsets (green) in *Chx10-Cre;Pcdh-γ*$^{fcon3/+}$ (control) and *Chx10-Cre;Pcdh-γ*$^{fcon3/fcon3}$ retinas. ChAT-positive processes ramify in sublaminae (S) 2 and 4, and vGlut3-positive processes ramify in S3. (**C**,**D**) Synaptotagmin 2 (SytII) -positive OFF bipolar processes (red) and Gγ13-positive ON bipolar processes (green) ramify in the outer and inner regions of the IPL, respectively. In all cases, laminar specificity is retained in mutants, but marker-laminae are reduced and disrupted. (**E**) Sketch of IPL sublaminae stained by the markers used in this study. Scale bars: 50 μm.

precisely patterned synaptic connectivity. We therefore monitored action potentials simultaneously from large populations of RGCs in control and Pcdh-γ mutant retinas, using a multi-electrode array (Meister et al., 1994). Results from *Chx10-Cre;Pcdh-γ*$^{fcon3/fcon3}$ retinas and peripheral regions of *Pax6α-Cre;Pcdh-γ*$^{fcon3/fcon3}$ retinas were similar, so they are combined here. We did not use *Pcdh-γ;Bax* double mutants for this study, because visual responses are compromised in *Bax* single mutants (Pequignot et al., 2003).

RGCs in Pcdh-γ mutant and control retinas showed a similar variety of responses to small flashing spots, including sustained and transient ON, OFF and ON-OFF responses (Fig. 9A).

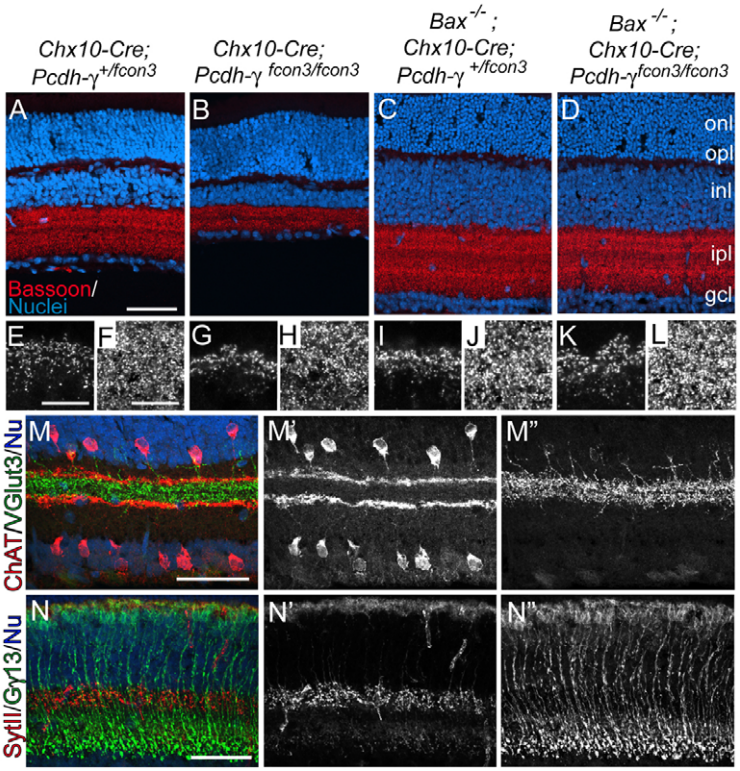

Fig. 8. Laminar specificity and synapse formation by Pcdh-γ-deficient neurons rescued from apoptosis. (**A-D**) Sections from retinas mutant for Bax (*Chx10-Cre;Pcdh-γ*$^{fcon3/+}$ *Bax*$^{-/-}$), Pcdh-γ (*Chx10-Cre;Pcdh-γ*$^{fcon3/fcon3}$ *Bax*$^{+/-}$), both (*Chx10-Cre;Pcdh-γ*$^{fcon3/fcon3}$ *Bax*$^{-/-}$) or neither (*Chx10-Cre;Pcdh-γ*$^{+/fcon3}$ *Bax*$^{+/-}$). Sections were stained with anti-bassoon (red) and Po-pro1 (blue). Thickness of IPL and INL are similar in *Bax* mutants and *Bax*, *Pcdh-γ* double mutants; both are thicker than those in *Pcdh-γ* mutants. (**E-L**) High power images of OPL (E,G,I,K) and IPL (F,H,J,L) from retinas in A-D. Density of synaptic puncta is similar in *Bax* mutants and *Bax*, *Pcdh-γ* double mutants (see Fig. S2 in the supplementary material for quantification). (**M**,**N**) *Chx10-Cre;Pcdh-γ*$^{fcon3/fcon3}$ *Bax*$^{-/-}$ mutants immunostained for ChAT (red) and vGluT3 (green) (M) or synaptotagmin 2 (SytII, red), and Gγ13 (green) (N). All processes make lamina-specific arbors (compare with Fig. 7) and disruptions seen in Pcdh-γ single mutants are absent in double mutants. Scale bars: 100 μm in A-D; 10 μm in E-L; 50 μM in M,N.

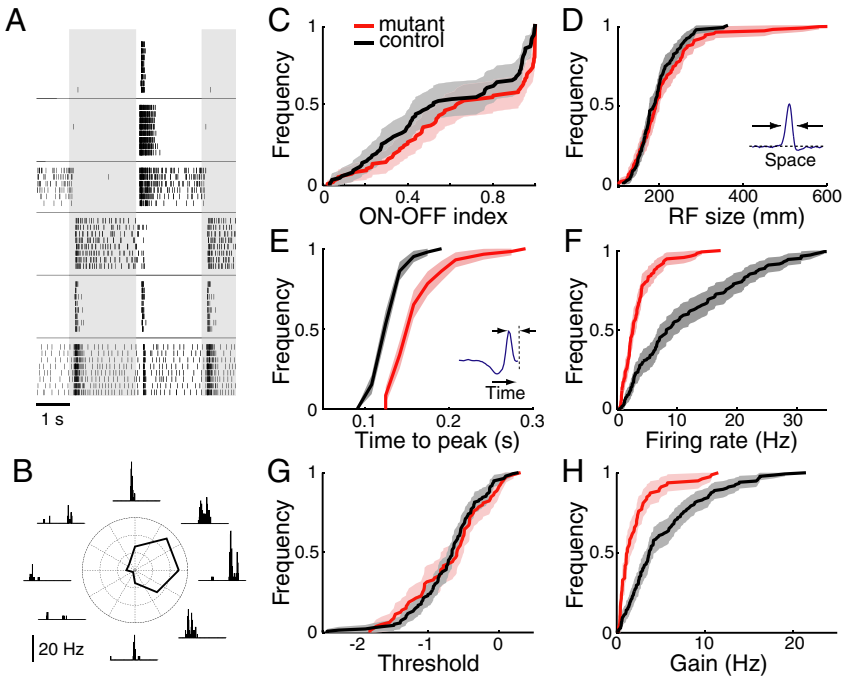

Fig. 9. Visual processing in Pcdh-γ mutant retina. (**A**) Visual responses of RGCs in Pcdh-γ mutant retina to a flashing spot at photopic intensities. Background shading indicates periods of light On and Off. Each panel is a raster graph of firing from one neuron; each row is a repeat of the same stimulus; tick marks represent action potentials. Neurons vary greatly in whether they respond to light onset or offset, and whether firing is transient or sustained after the switch. (**B**) Direction-selective response of an RGC in Pcdh-γ mutant retina to a grating stimulus moving in eight different directions. Insets are histograms of spike times during one period of the grating (wavelength 664 μm, speed 664 μm/s). The polar plot reports the average firing rate as a function of direction. (**C-H**) Distribution of response parameters in mutant and control retinas. Each panel inspects a different characteristic of the visual response, and plots a cumulative histogram of that quantity for RGCs in mutant retinas (red curve, 115 cells, *Chx10-Cre;Pcdh-γ*$^{fcon3/fcon3}$ or the peripheral region of the *Pax6α-Cre;Pcdh-γ*$^{fcon3/fcon3}$) and control retinas (black curve, 143 cells, genotype *Pax6α-Cre;Pcdh-γ*$^{+/fcon3}$ or *Pcdh-γ*$^{fcon3/fcon3}$). The shaded range indicates 95% confidence interval. (C) Ratio of On and Off responses in mutant and control retinas. For each cell we computed an On-Off index from the experiment in A: (number of spikes fired during the on-phase of the spot)/(total number of spikes fired). (D) Size of the receptive field center, measured as the full width at half maximum of the receptive field profile $b(x)$ (inset, see Eqn 2). (E) Speed of the response, measured as the time to peak of the temporal integration function $a(t)$ (inset, see Eqn 2). (F) Average firing rate observed during stimulation with flickering gratings. (G,H) Threshold (G) and gain (H) of responses in a linear-nonlinear model (see Eqn 3).

Proportions of ON- and OFF-dominated responses were identical in mutants and controls (Fig. 9C). Mutant RGCs responded to very dim flashes, which excite only rods, and also to bright flashes, which predominantly excite cones (data not shown), indicating that both rod- and cone-activated pathways were functional. We also probed the retina with moving bars and gratings to elicit direction-selective responses, which are known to depend on specific patterns of connectivity in the IPL (Masland, 2001). Both ON and ON-OFF direction-selective cells were encountered in mutant retinas (Fig. 9B; data not shown). Some control and mutant RGCs had receptive field surrounds, where light has the opposite effect of the center (see Fig. S3 in the supplementary material), indicating that lateral inhibitory connections are functional in these circuits.

To survey response properties quantitatively, we stimulated the retina with randomly flickering bars and applied a reverse correlation method (Chichilnisky, 2001; Meister et al., 1994). This measures spatio-temporal receptive fields, revealing how RGCs respond to light intensity at different points on the retina and at different times in the past (see Fig. S3 in the supplementary material). The size of the receptive field center varied greatly among RGCs, but the distribution was similar in control and mutant retinas (Fig. 9D). However, the time course of the light response was significantly slower in mutant retina (Fig. 9E). Moreover, mutant RGCs fired at much lower rates in response to flicker stimuli (Fig. 9F). In principle, this could result from an elevated response threshold; alternatively, the gain of the response might be lower once the threshold is crossed. Based on fitting with a linear-nonlinear model (Chichilnisky, 2001), we found that the threshold is unaltered, but the gain is reduced in mutants (Fig. 9G-H).

DISCUSSION

Protocadherins and neural specificity

Interest in the clustered protocadherins has centered on the tantalizing idea that their molecular diversity may underlie the extraordinary synaptic specificity of the brain (Benson et al., 2001; Hamada and Yagi, 2001; Hirayama and Yagi, 2006; Kohmura et al., 1998; Morishita and Yagi, 2007; Serafini, 1999; Shapiro and Colman, 1999; Washbourne et al., 2004; Wu and Maniatis, 1999; Yagi and Takeichi, 2000). Several observations that led to this notion are summarized in the Introduction. Moreover, Hasegawa et al. (Hasegawa et al., 2008) recently showed that olfactory axons bearing a single type of odorant receptor fail to coalesce properly onto glomeruli in olfactory bulbs of mice lacking Pcdh-α genes.

These considerations, coupled with the finding that most retinal cells express Pcdh-γ genes, led us to expect that retinal circuitry might be grossly defective in their absence. Surprisingly, it was not. Synaptic specializations were present in the OPL and IPL of *Pcdh-γ* mutants, and the light-responsiveness of RGCs indicates that synapses in both laminae were functional. Moreover, synapses in the IPL were sublamina specific as judged by distribution of arbors. This distribution provides a stringent test of targeting, in that 10 or more IPL sublaminae are separated by only a few tens of micrometers (Roska and Werblin, 2001; Wässle, 2004).

The loss of neurons in Pcdh-γ-deficient retinas potentially complicates this interpretation: neurons making improper arbors or connections could be selectively eliminated, so only neurons that wired up properly would be retained. The ability to block apoptosis in Pcdh-γ mutant retinas by deleting the *Bax* gene allowed us to test this possibility. Lamina-specific targeting was, if anything, more precise in the absence of *Bax* than in its presence, in that disruptions and irregularities seen in *Pcdh-γ*$^{-/-}$ laminae were absent in double mutants. Therefore, IPL disruptions observed in *Pcdh-γ*$^{-/-}$ retinas presumably reflected loss of cells rather than mistargeting of neurites. Moreover, with apoptosis prevented by *Bax* deletion, loss of Pcdh had no detectable effect on the number of synapses in either the IPL or the OPL.

The ability of mutant retinas to process visual information was also remarkably preserved. RGCs exhibited a wide range of complex responses, and their receptive field sizes were normal. Because the spatial extent of RGC receptive field centers are largely determined by their dendritic fields, which collect input from bipolar cells (Wässle, 2004), this result suggests that mutant RGC arbors are normal in size. As bipolar cells provide the main excitation to RGCs, their decreased number could account for the lower firing rate and response gain in mutant RGCs. Most likely to result from lack of Pcdh-γ rather than from decreased cell number are the defects in response dynamics, which are controlled by synaptic properties in the OPL (DeVries, 2000) and IPL (Nirenberg and Meister, 1997). One way to distinguish which defects are due to loss of interneurons and altered ratios of cell types and which to loss of Pcdh-γ genes per se will be to record from retinas lacking both Pcdh-γ genes and Bax. This work is under way, but is complicated by the fact that naturally occurring cell death is also blocked by *Bax* deletion, and that visual responses are compromised in these mutants (Pequignot et al., 2003).

Synaptic circuitry and neuronal survival

Patterns of apoptosis in Pcdh-γ-deficient retina are similar to those in spinal cord (Wang et al., 2002; Weiner et al., 2005) (see also Prasad et al., 2008) in several respects. First, approximately half of the interneurons in each region are lost in the absence of Pcdh-γ genes. Second, some interneuronal subtypes and primary sensory neurons (dorsal root ganglion cells and photoreceptors) are spared in both regions, even though they express *Pcdh-γ* genes. Third, the loss of neurons in Pcdh-γ mutants occurs during the period of naturally occurring cell death. One apparent difference is that the output neurons of the spinal cord, motoneurons, are spared in Pcdh-γ-deficient mice, whereas those of retina, RGCs, are affected. However, at least some apoptosis of RGCs is cell-nonautonomous, reflecting either loss of Pcdh-γ from presynaptic cells or loss of input cells themselves. It is possible that in the mutants analyzed to date, motoneurons retain a larger fraction of their inputs than do RGCs, and that this contributes to their survival.

Retina and spinal cord phenotypes are also similar in that loss of Pcdh-γ genes leads to decreased numbers of synapses in both tissues. In spinal cord, synapse loss does not result simply from neuron loss, as shown by analysis of Pcdh-γ-deficient mice in which apoptosis was blocked: neuronal number was normal in these animals, but synapse number was still reduced (Weiner et al., 2005). This result is consistent with the idea that failure of synapse formation or function impairs neuronal survival (see also Prasad et al., 2008). In fact, complete blockade of synaptic function in embryonic brain leads to increased apoptosis (Verhage et al., 2000). By contrast, deletion of Pcdh-γ in a *Bax*$^{-/-}$ background does not decrease synapse density in retina. In addition, given the electrophysiological evidence for maintained synaptic function, it seems unlikely that any synaptic defect is sufficient in magnitude to explain the massive apoptosis we observe. Likewise, synaptic patterns in the IPL of Pcdh-γ mutants are at least as well preserved in the absence of Bax as in its presence, ruling out the possibility that apoptosis reflects selective elimination of inappropriate synapses.

Thus, synapses can be lost in the absence of neuronal loss in the spinal cord, and neurons can be lost in the absence of major synaptic defects in retina. These results suggest that Pcdh-γ regulates neuronal survival and synaptic maturation by distinct mechanisms, and that effects on these two processes differ in severity among brain regions. The combinatorial diversity provided by the Pcdh-γ genes may therefore be useful for selectively controlling the size of diverse neuronal populations.

We thank Joshua Weiner for sharing data. This work was supported by grants from the National Institutes of Health to M.M. and J.R.S, a NARSAD Young Investigator award to J.L., and Damon Runyon Cancer Research Foundation Fellowship to Y.-F.Z.

Supplementary material

Supplementary material for this article is available at http://dev.biologists.org/cgi/content/full/135/24/4141/DC1

References

Benson, D. L., Colman, D. R. and Huntley, G. W. (2001). Molecules, maps and synapse specificity. *Nat. Rev. Neurosci.* **2**, 899-909.

Blanks, J. C., Hageman, G. S. and Johnson, L. V. (1987). Appearance of PNA-binding cells within the outer nuclear layer coinciding with photoreceptor degeneration in rd mice. *Prog. Clin. Biol. Res.* **247**, 229-242.

Chichilnisky, E. J. (2001). A simple white noise analysis of neuronal light responses. *Network* **12**, 199-213.

DeVries, S. H. (2000). Bipolar cells use kainate and AMPA receptors to filter visual information into separate channels. *Neuron* **28**, 847-856.

Esumi, S., Kakazu, N., Taguchi, Y., Hirayama, T., Sasaki, A., Hirabayashi, T., Koide, T., Kitsukawa, T., Hamada, S. and Yagi, T. (2005). Monoallelic yet combinatorial expression of variable exons of the protocadherin-alpha gene cluster in single neurons. *Nat. Genet.* **37**, 171-176.

Farah, M. H. and Easter, S. S., Jr (2005). Cell birth and death in the mouse retinal ganglion cell layer. *J. Comp. Neurol.* **489**, 120-134.

Frank, M., Ebert, M., Shan, W., Phillips, G. R., Arndt, K., Colman, D. R. and Kemler, R. (2005). Differential expression of individual gamma-protocadherins during mouse brain development. *Mol. Cell. Neurosci.* **29**, 603-616.

Ghosh, K. K., Bujan, S., Haverkamp, S., Feigenspan, A. and Wässle, H. (2004). Types of bipolar cells in the mouse retina. *J. Comp. Neurol.* **469**, 70-82.

Goldberg, J. L., Klassen, M. P., Hua, Y. and Barres, B. A. (2002). Amacrine-signaled loss of intrinsic axon growth ability by retinal ganglion cells. *Science* **296**, 1860-1864.

Hamada, S. and Yagi, T. (2001). The cadherin-related neuronal receptor family: a novel diversified cadherin family at the synapse. *Neurosci. Res.* **41**, 207-215.

Hasegawa, S., Hamada, S., Kumode, Y., Esumi, S., Katori, S., Fukuda, E., Uchiyama, Y., Hirabayashi, T., Mombaerts, P. and Yagi, T. (2008). The protocadherin-alpha family is involved in axonal coalescence of olfactory sensory neurons into glomeruli of the olfactory bulb in mouse. *Mol. Cell. Neurosci.* **38**, 66-79.

Haverkamp, S. and Wässle, H. (2000). Immunocytochemical analysis of the mouse retina. *J. Comp. Neurol.* **424**, 1-23.

Haverkamp, S., Ghosh, K. K., Hirano, A. A. and Wässle, H. (2003). Immunocytochemical description of five bipolar cell types of the mouse retina. *J. Comp. Neurol.* **455**, 463-476.

Hill, E., Broadbent, I. D., Chothia, C. and Pettitt, J. (2001). Cadherin superfamily proteins in Caenorhabditis elegans and Drosophila melanogaster. *J. Mol. Biol.* **305**, 1011-1024.

Hirayama, T. and Yagi, T. (2006). The role and expression of the protocadherin-alpha clusters in the CNS. *Curr. Opin. Neurobiol.* **16**, 336-342.
Huang, L., Max, M., Margolskee, R. F., Su, H., Masland, R. H. and Euler, T. (2003). G protein subunit G gamma 13 is coexpressed with G alpha o, G beta 3, and G beta 4 in retinal ON bipolar cells. *J. Comp. Neurol.* **455**, 1-10.
Kim, I. J., Zhang, Y., Yamagata, M., Meister, M. and Sanes, J. R. (2008). Molecular identification of a retinal cell type that responds to upward motion. *Nature* **452**, 478-482.
Knudson, C. M., Tung, K. S., Tourtellotte, W. G., Brown, G. A. and Korsmeyer, S. J. (1995). Bax-deficient mice with lymphoid hyperplasia and male germ cell death. *Science* **270**, 96-99.
Kohmura, N., Senzaki, K., Hamada, S., Kai, N., Yasuda, R., Watanabe, M., Ishii, H., Yasuda, M., Mishina, M. and Yagi, T. (1998). Diversity revealed by a novel family of cadherins expressed in neurons at a synaptic complex. *Neuron* **20**, 1137-1151.
Koulen, P., Fletcher, E. L., Craven, S. E., Bredt, D. S. and Wässle, H. (1998). Immunocytochemical localization of the postsynaptic density protein PSD-95 in the mammalian retina. *J. Neurosci.* **18**, 10136-10149.
Lewandoski, M., Meyers, E. N. and Martin, G. R. (1997). Analysis of Fgf8 gene function in vertebrate development. *Cold Spring Harb. Symp. Quant. Biol.* **62**, 159-168.
Marquardt, T., Ashery-Padan, R., Andrejewski, N., Scardigli, R., Guillemot, F. and Gruss, P. (2001). Pax6 is required for the multipotent state of retinal progenitor cells. *Cell* **105**, 43-55.
Masland, R. H. (2001). The fundamental plan of the retina. *Nat. Neurosci.* **4**, 877-886.
Meister, M., Pine, J. and Baylor, D. A. (1994). Multi-neuronal signals from the retina: acquisition and analysis. *J. Neurosci. Methods* **51**, 95-106.
Meyer-Franke, A., Kaplan, M. R., Pfrieger, F. W. and Barres, B. A. (1995). Characterization of the signaling interactions that promote the survival and growth of developing retinal ganglion cells in culture. *Neuron* **15**, 805-819.
Morishita, H. and Yagi, T. (2007). Protocadherin family: diversity, structure, and function. *Curr. Opin. Cell Biol.* **19**, 584-592.
Mosinger Ogilvie, J., Deckwerth, T. L., Knudson, C. M. and Korsmeyer, S. J. (1998). Suppression of developmental retinal cell death but not of photoreceptor degeneration in Bax-deficient mice. *Invest. Ophthalmol. Vis. Sci.* **39**, 1713-1720.
Nirenberg, S. and Meister, M. (1997). The light response of retinal ganglion cells is truncated by a displaced amacrine circuit. *Neuron* **18**, 637-650.
Noonan, J. P., Grimwood, J., Schmutz, J., Dickson, M. and Myers, R. M. (2004). Gene conversion and the evolution of protocadherin gene cluster diversity. *Genome Res.* **14**, 354-366.
Novak, A., Guo, C., Yang, W., Nagy, A. and Lobe, C. G. (2000). Z/EG, a double reporter mouse line that expresses enhanced green fluorescent protein upon Cre-mediated excision. *Genesis* **28**, 147-155.
Obata, S., Sago, H., Mori, N., Davidson, M., St John, T. and Suzuki, S. T. (1998). A common protocadherin tail: multiple protocadherins share the same sequence in their cytoplasmic domains and are expressed in different regions of brain. *Cell Adhes. Commun.* **6**, 323-333.
Pang, J. J., Gao, F. and Wu, S. M. (2002). Segregation and integration of visual channels: layer-by-layer computation of ON-OFF signals by amacrine cell dendrites. *J. Neurosci.* **22**, 4693-4701.
Pequignot, M. O., Provost, A. C., Salle, S., Taupin, P., Sainton, K. M., Marchant, D., Martinou, J. C., Ameisen, J. C., Jais, J. P. and Abitbol, M. (2003). Major role of BAX in apoptosis during retinal development and in establishment of a functional postnatal retina. *Dev. Dyn.* **228**, 231-238.
Phillips, G. R., Tanaka, H., Frank, M., Elste, A., Fidler, L., Benson, D. L. and Colman, D. R. (2003). Gamma-protocadherins are targeted to subsets of synapses and intracellular organelles in neurons. *J. Neurosci.* **23**, 5096-5104.
Prasad, T., Wang, X., Gray, P. A. and Weiner, J. A. (2008). A differential developmental pattern of spinal interneuron apoptosis during synaptogenesis: insights from genetic analyses of the protocadherin-γ gene cluster. *Development* **135**, 4153-4164.
Roska, B. and Werblin, F. (2001). Vertical interactions across ten parallel, stacked representations in the mammalian retina. *Nature* **410**, 583-587.
Rowan, S. and Cepko, C. L. (2004). Genetic analysis of the homeodomain transcription factor Chx10 in the retina using a novel multifunctional BAC transgenic mouse reporter. *Dev. Biol.* **271**, 388-402.
Serafini, T. (1999). Finding a partner in a crowd: neuronal diversity and synaptogenesis. *Cell* **98**, 133-136.
Shapiro, L. and Colman, D. R. (1999). The diversity of cadherins and implications for a synaptic adhesive code in the CNS. *Neuron* **23**, 427-430.
Sharma, R. K., O'Leary, T. E., Fields, C. M. and Johnson, D. A. (2003). Development of the outer retina in the mouse. *Brain Res. Dev. Brain Res.* **145**, 93-105.
Stacy, R. C., Demas, J., Burgess, R. W., Sanes, J. R. and Wong, R. O. (2005). Disruption and recovery of patterned retinal activity in the absence of acetylcholine. *J. Neurosci.* **25**, 9347-9357.
Takeichi, M. (2007). The cadherin superfamily in neuronal connections and interactions. *Nat. Rev. Neurosci.* **8**, 11-20.
tom Dieck, S. and Brandstätter, J. H. (2006). Ribbon synapses of the retina. *Cell Tissue Res.* **326**, 339-346.
Verhage, M., Maia, A. S., Plomp, J. J., Brussaard, A. B., Heeroma, J. H., Vermeer, H., Toonen, R. F., Hammer, R. E., van den Berg, T. K., Missler, M. et al. (2000). Synaptic assembly of the brain in the absence of neurotransmitter secretion. *Science* **287**, 864-869.
Wahlin, K. J., Lim, L., Grice, E. A., Campochiaro, P. A., Zack, D. J. and Adler, R. (2004). A method for analysis of gene expression in isolated mouse photoreceptor and Muller cells. *Mol. Vis.* **10**, 366-375.
Wang, X., Weiner, J. A., Levi, S., Craig, A. M., Bradley, A. and Sanes, J. R. (2002). Gamma protocadherins are required for survival of spinal interneurons. *Neuron* **36**, 843-854.
Washbourne, P., Dityatev, A., Scheiffele, P., Biederer, T., Weiner, J. A., Christopherson, K. S. and El-Husseini, A. (2004). Cell adhesion molecules in synapse formation. *J. Neurosci.* **24**, 9244-9249.
Wässle, H. (2004). Parallel processing in the mammalian retina. *Nat. Rev. Neurosci.* **5**, 747-757.
Weiner, J. A., Wang, X., Tapia, J. C. and Sanes, J. R. (2005). Gamma protocadherins are required for synaptic development in the spinal cord. *Proc. Natl. Acad. Sci. USA* **102**, 8-14.
White, F. A., Keller-Peck, C. R., Knudson, C. M., Korsmeyer, S. J. and Snider, W. D. (1998). Widespread elimination of naturally occurring neuronal death in Bax-deficient mice. *J. Neurosci.* **18**, 1428-1439.
Wu, Q. and Maniatis, T. (1999). A striking organization of a large family of human neural cadherin-like cell adhesion genes. *Cell* **97**, 779-790.
Wu, Q. and Maniatis, T. (2000). Large exons encoding multiple ectodomains are a characteristic feature of protocadherin genes. *Proc. Natl. Acad. Sci. USA* **97**, 3124-3129.
Yagi, T. and Takeichi, M. (2000). Cadherin superfamily genes: functions, genomic organization, and neurologic diversity. *Genes Dev.* **14**, 1169-1180.
Yamagata, M. and Sanes, J. R. (2008). Dscam and Sidekick proteins direct lamina-specific synaptic connections in vertebrate retina. *Nature* **451**, 465-469.
Young, R. W. (1984). Cell death during differentiation of the retina in the mouse. *J. Comp. Neurol.* **229**, 362-373.
Zhang, J., Gray, J., Wu, L., Leone, G., Rowan, S., Cepko, C. L., Zhu, X., Craft, C. M. and Dyer, M. A. (2004). Rb regulates proliferation and rod photoreceptor development in the mouse retina. *Nat. Genet.* **36**, 351-360.
Zou, C., Huang, W., Ying, G. and Wu, Q. (2007). Sequence analysis and expression mapping of the rat clustered protocadherin gene repertoires. *Neuroscience* **144**, 579-603.

γ-Protocadherins regulate neuronal survival but are dispensable for circuit formation in retina

DEV027912 Supplementary Material

Files in this Data Supplement:

- **Supplemental Figure S1** -

Fig. S1. Chx10-Cre recombination pattern in the retina. (**A**,**B**) Retina sections of *Chx10-Cre; Z/EG* P7 mice illustrate Chx10-CreGFP mediated recombination pattern, in which recombined cells express GFP (green) due to excision of the stop translation sequence in the *Z/EG* transgene. Unrecombined cells express *lacZ* and are immunolabeled for *β*-galactosidase (red). In *Chx10-Cre; Z/EG* retinas, the majority of retinal cells are descendents of progenitors that have undergone Cre-mediated recombination. However, occasional columns of cells spanning all layers and roughly half the cells present in the GCL are unrecombined (red; closed arrowhead). Chx10-CreGFP is also expressed postnatally in bipolar cells (A,D,E; green, open arrow). (B) Co-immunolabeling of *Chx10-Cre; Z/EG* retinas with GFP (green) and Brn3a (magenta) reveal that although many RGCs are spared, some RGCs are recombined (double arrow). (**C-E**) Immunostaining of GFP in retina sections of *Pcdh-γ* $^{fcon3/fcon3}$, *Chx-10-Cre;Pcdh-γ* $^{fcon3/fcon3}$ and *Chx-10-Cre;Pcdh-γ* $^{fdel/fdel}$ P18 mice report the extent of *Pcdh-γ* excision. In *Pcdh-γ* $^{fcon3/fcon3}$ retinas, Pcdh-γ-GFP fusion proteins are present throughout the retina (C). In *Chx-10-Cre;Pcdh-γ* $^{fcon3/fcon3}$ and *Chx-10-Cre;Pcdh-γ* $^{fdel/fdel}$ retinas, Pcdh-γ-GFP fusion proteins are dramatically reduced, with the exception of thin stripes of GFP sparsely and variably distributed throughout the mutant retinas (detected in the outersegment and ONL; closed arrowhead). GFP in the INL reflects postnatal GFP expression of Chx10-CreGFP transgene (D,E, open arrow). Scale bar: 50 μm.

- **Supplemental Figure S2** -

Fig. S2. Synaptic puncta density is similar in *Pcdh-γ; Bax* double mutant and control retinas. (**A**,**B**) Quantification of PNA-labeled cone pedicles and bassoon-immunolabeled puncta in the OPL of control and *Chx10-Cre; Pcdh-γ*$^{fcon3/fcon3}$; *Bax*$^{-/-}$ retina sections of P28 mice. Bars show mean±s.e.m. of 15-18 microscope fields from three double mutant animals (red bars) and three control siblings (black bars; two *Chx10-Cre; Pcdh-γ* $^{+/fcon3}$; *Bax*$^{-/-}$ and one *Pcdh-γ* $^{+/fcon3}$; *Bax*$^{-/-}$ animals). Numbers of PNA-labeled pedicles (A) and Bassoon-positive puncta per unit area (B, left), and total Bassoon-positive puncta area (B, right) did not differ in double mutants compared to controls (by Student's t-test). (**C**) Cumulative histogram of Bassoon labeled puncta sizes in the OPL of double mutants compared with controls shows that they did not differ in their distribution (over 900 puncta analyzed for each; Kolmogorov-Smirnov test). (**D**) Quantification of Bassoon-immunolabeled puncta in the IPL of control and *Chx10-Cre; Pcdh-γ*$^{fcon3/fcon3}$; *Bax*$^{-/-}$ retina sections of P28 mice. Bars show mean±s.e.m. of 13-15 microscope fields at similar regions of OFF and ON lamina of the IPL of three double mutant animals and control siblings (as above). The number (left) and total puncta area (right) did not differ between *Pcdh-γ; Bax* double mutants and controls (by ANOVA). (**E**) Cumulative histogram of bassoon puncta sizes in the IPL shows similar distributions in double mutants and controls (over 3700 puncta analyzed for each; Kolmogorov-Smirnov test).

- **Supplemental Figure S3** -

Fig. S3. Spatio-temporal receptive fields for a sample of ganglion cells in mutant and control retinas. Each panel displays the spike-triggered average stimulus of one neuron, $h(x,t)$ (as defined in Eqn 1). Within such a receptive field, the right-most 'blob' indicates the response polarity of the receptive field center: red for ON-cells, blue for OFF cells. In some cases (asterisks) one can see regions above and below the center with the opposite polarity. These reflect the antagonistic surround of the receptive field. For further interpretation of such receptive fields, see also Kim et al. (Kim et al., 2008).

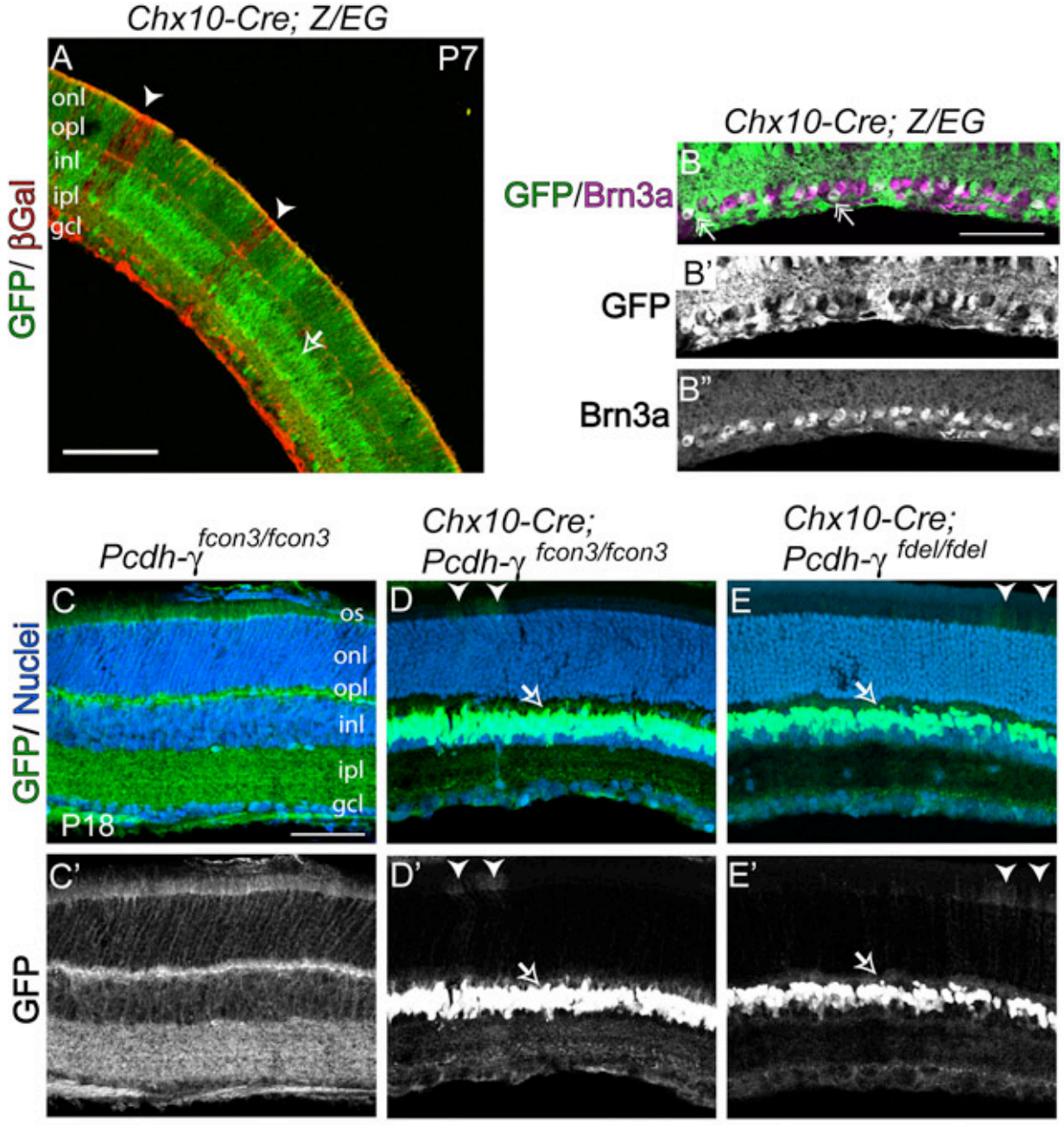
Chx10-Cre; Z/EG
A
P7
onl
opl
inl
ipl
gcl
GFP/ βGal
Chx10-Cre; Z/EG
B
GFP/Brn3a
B'
GFP
B"
Brn3a
Pcdh-γ fcon3/fcon3
Chx10-Cre; Pcdh-γ fcon3/fcon3
Chx10-Cre; Pcdh-γ fdel/fdel
C
os
onl
opl
inl
ipl
gcl
P18
GFP/ Nuclei
D
E
C'
D'
E'
GFP

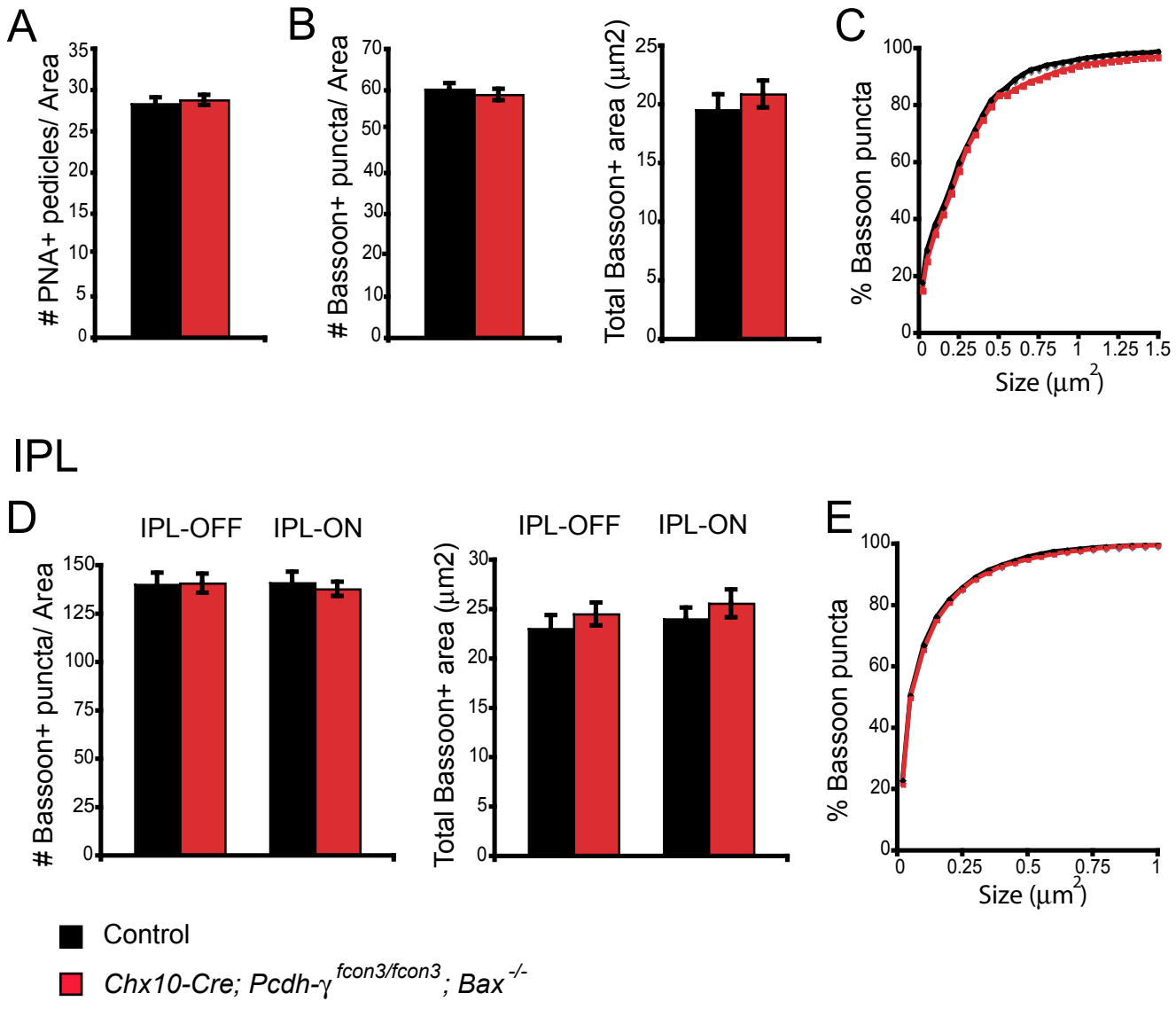
OPL
A
PNA+ pedicles/ Area
0
5
10
15
20
25
30
35
B
Bassoon+ puncta/ Area
0
10
20
30
40
50
60
70
Total Bassoon+ area (µm2)
0
5
10
15
20
25
C
% Bassoon puncta
0
20
40
60
80
100
0 0.25 0.5 0.75 1 1.25 1.5
Size (µm2)
IPL
D
IPL-OFF
IPL-ON
Bassoon+ puncta/ Area
0
25
50
75
100
125
150
IPL-OFF
IPL-ON
Total Bassoon+ area (µm2)
0
5
10
15
20
25
30
E
% Bassoon puncta
0
20
40
60
80
100
0 0.25 0.5 0.75 1
Size (µm2)
Control
Chx10-Cre; Pcdh-γ fcon3/fcon3; Bax -/-

Mutant

Control

position(mm)

1
2
3
4
5

-1 -0.5 0

time (s)

1

-1